Combined Application of LEED and STM in Surface Crystallography†

Klaus Heinz* and Lutz Hammer

Lehrstuhl für Festkörperphysik, Universität Erlangen-Nürnberg, Staudtstrasse 7, D-91058 Erlangen, Germany

Received: February 17, 2004; In Final Form: April 20, 2004

The power of the combined application of quantitative low-energy electron diffraction (LEED) and scanning tunneling microscopy (STM) is demonstrated for several examples. It is shown that the STM image in most cases provides the key to the applicable structural model type. Such an initial guess is needed by LEED to start a structural search in which the model parameters are varied so that the complete crystallographic structure is obtained. The input from STM is invaluable when a large number of different model types have to be tested or, even more, in cases where the scientist lacks the imagination to think of the correct model type. If a structural misinterpretation of the STM image puts LEED on the wrong track, then the method becomes aware of that by the best fit achieved being unsatisfying. In this sense, the combination of STM and quantitative LEED is almost ideal and provides new power for the access of complex structures.

1. LEED and STM as Singly and Jointly Applied Techniques

Quantitative low-energy electron diffraction (LEED) and scanning tunneling microscopy (STM) are well-known surface techniques that are reliably and impressively applied in a huge number of cases. Both are capable of retrieving surface atomic positions, however, by different ways and to a very different extent and precision. Whereas STM works directly in real space, LEED is a reciprocal space technique and requires the full dynamical analysis of measured spot intensities, which usually exceeds the efforts of the measurement. LEED electrons, typically in an energy range of about 20−600 eV, penetrate the surface by about 1 nm and so are sensitive to the atomic positions within a small number of surface layers. In contrast, STM probes the electronic density of states at the surface rather than at atomic positions. It is only by the correlation between electronic and geometrical properties that information about the positions is provided via the STM image. As in most cases, this correlation is to some extent uncertain; there is also usually some uncertainty about the atomic coordinates, which can be up to the order of 50 pm. When there are different chemical species within the surface, their vertical positions appearing in the STM image must not coincide with their true ones. In the case of corrugated surfaces decorated with adsorbates, there can also be lateral deviations, as has been proven recently (e.g., the case of Fe/Ir(100) using first principles calculations[1] in comparison to STM images[2]). With the tip structure involved in the scanning of the surface, additional image distortions might occur, whereby atoms can even be missing or ghost atoms can appear. Tip−surface interactions can also add to deviations from the true structure.

However, the scattering of LEED electrons is largely dominated by the atomic nucleus and the core electrons, so LEED is sensitive to the atomic positions. The spatial distribution of valence or conduction electrons is rather unimportant: the electronic structure enters only by electronic excitations caused by the incident beam, limiting its penetration depth. Yet because only intensities rather than diffraction amplitudes are measured, a trial-and-error method has to be applied to retrieve the atomic positions. This is substantially complicated by the usually strong multiple scattering so that even the Fourier transform of intensities fails to reproduce the Patterson function. Direct evaluation techniques (e.g., holographic inversion including maximum entropy methods[3]) have been successful only in a few cases. (For a survey, see the special volume in ref 4.) Instead, one needs to assume a crystallographic model of the surface and then calculate the corresponding intensities, compare them with the experimental data, and repeat this procedure by modifying the atomic coordinates until the comparison is favorable. The payback of these computational efforts is a structural precision that often is in the picometer range. Yet, though successful in many cases[5] and though sophisticated structural search procedures and computational methods are applied (for a review see ref 6), the method is applicable only if the type of surface model is known so that atomic coordinates are defined and can be varied in the structural search. Frequently, different model types consistent with the symmetry of the diffraction pattern must be tested because LEED provides no beforehand selection. For complex structures, the number of possible models to be tested grows beyond practical limits. Even more, the scientist may lack the necessary imagination for the correct model, and the intensity data, if ever measured, remain in the drawer.

This is the point where the combined application of LEED and STM provides new power. The STM image yields at least an idea of the atomic positions in the top surface layer without the need for picometer precision. Because the bulk of the sample and the surface orientation are always known, there is a also good chance of extending the structural idea provided by STM to deeper layers so that the correct model type can be derived. Then the usual structural search procedure can be applied. Of course, the surface needs to be in the same state when investigated by STM and LEED. This puts some demands on the UHV equipment. Usually two stages within one vessel are necessary with sample transfer provided. Also, experimental expertise in both techniques must be available in the same laboratory, in particular, the achievement of atomic resolution

† Part of the special issue "Gerhard Ertl Festschrift".

* Corresponding author. E-mail: kheinz@fkp.physik.uni-erlangen.de.

10.1021/jp049289n CCC: $27.50
Published on Web 06/08/2004

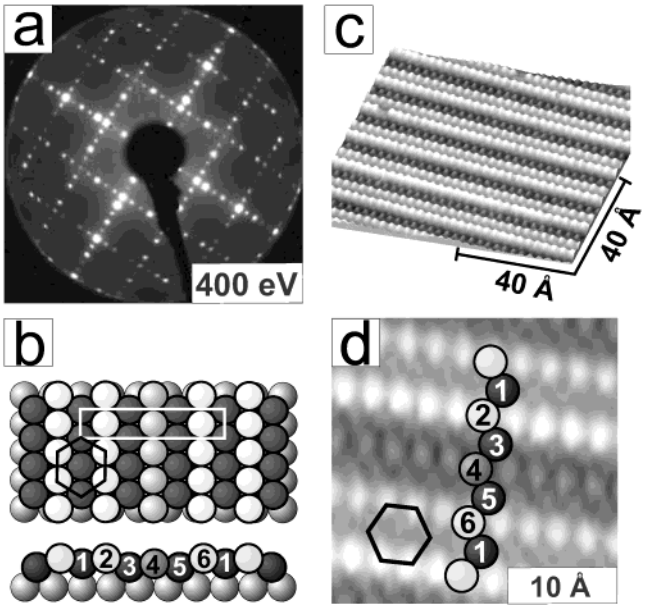

Figure 1. (a) LEED diffraction pattern and (b) ball model in top and side views of Ir(100)-(5 × 1)-hex. On the right, atomically resolved STM images are displayed in perspective (c) and the top (d) view with, in the latter case, reference to the row numbering given in panel b.

in STM and the measurement of high-precision and low-noise data for a precise angular alignment of the sample in LEED. This must be complemented by a theoretical subgroup for the intensity analysis. These restrictions may be the reason that the almost ideal combination of STM and LEED is not widely implemented.

In the following text, we demonstrate the described power of combined STM and LEED by several examples. We concentrate on examples using the same substrate (i.e., Ir(100)). Even its clean surface structure is by no means trivial, and we demonstrate at the beginning that the extraction of the correct model from the STM image is not always simple. We then proceed to Ir(100) as restructured upon hydrogen adsorption and eventually consider the epitaxial growth of iron on this phase. All surfaces presented exhibit a superstructure that is large enough to allow for comparably complex structures. For the LEED measurements, homemade LEED optics were used. The intensity data were taken by a computer-controlled video camera from the luminescent screen.[6] Their analyses were carried out using the Erlangen program package, which applies the perturbation method TensorLEED.[7] STM images were taken with a commercial beetle-type scan head (RHK) with the sample always at room temperature.

2. Clean Ir(100) Surface

The (100) surface of iridium is one of the earliest "interesting" surfaces investigated by, at the time, nonquantitative LEED.[8] Interesting means that its diffraction pattern does not exhibit (1 × 1) symmetry as should be expected for a bulk terminated fcc crystal but instead shows (5 × 1) symmetry as displayed in Figure 1a. The pattern was proposed to be generated by a reconstructed, quasi-hexagonally close-packed surface layer arranged on the unreconstructed bulk leading to the notation Ir(100)-(5 × 1)-hex for this surface phase. The unit mesh contains six surface atoms corresponding to a 20% higher atomic density in the top layer compared to that in the (100) layers below. Quantitative confirmation of the model by LEED had to wait until the 1980s.[9−12] Then the registry of the hexagonal overlayer with respect to the substrate was also determined as displayed in the top panel of Figure 1b with the unit mesh and the surface hexagon indicated.

Surprisingly, at first glance a high-resolution STM image does not exhibit a hexagonal top layer but a chainlike structure as shown in Figure 1c, highlighting a potential pitfall. This is because the top layer is substantially buckled (amplitude 0.5 Å) as displayed in the bottom panel of Figure 1b. Only the three most surface protruding atomic rows are imaged as illustrated in Figure 1d (representative atom numbers 2, 4, and 6). The tip fails to resolve deeper-lying atoms of the top layer so that half of the hexagonally arranged surface atoms are hidden. This demonstrates that complete atomic imaging of a surface is by no means trivial and must not be generally expected. In the present case and imagining that the structure of Ir(100)-(5 × 1)-hex had not been known by the arrival of STM, one might have derived a surface chain model with atomic rows 1, 3, and 5 missing. A LEED analysis based on such a model would never have resulted in a satisfying theory−experiment fit, yet despite this pitfall, the features displayed in STM (i.e., the density and arrangement of close-packed atomic chains) are reliable and rule out a huge number of other possible models accounting for the observed symmetric diffraction pattern. The lateral spacing of the chains is $^{3a}/_{5}$, with $a = 2.72$ Å being the nearest-neighbor spacing of Ir atoms in the bulk. This means that the chains cannot reside in equivalent sites of the quadratically ordered substrate, which by some way of thinking would certainly have led to the quasi-hexagonal model (with quasi indicating that the angles differ slightly from the ideal 60° value and that the surface is buckled). Also, with two atoms in the unit cell protruding strongly from the surface, STM provides information about the registry of the hexagonal overlayer with respect to the quadratic substrate.

Yet, what the STM image completely hides is the structure of deeper layers. Because of the misfit between a quadratically and hexagonally ordered layer and their interaction, it would be surprising if only the top layer is distorted. Only a surface-penetrating technique can provide information about this issue. In fact, some buckling of the second layer has been revealed recently by quantitative LEED.[13] Even more, by using electrons with energies up to 600 eV with their increased sensitivity to deeper layers (because of reduced attenuation), it has been shown that the distortion proceeds deep into the surface and is nonnegligible even in the fourth layer.[14] This is illustrated in Figure 2a, which also defines the corresponding structural parameters that were varied in the structural search. (Note that atoms 2/6 and 3/5 denoted in Figure 2b are symmetrically equivalent.) The quantitative LEED analysis results in an excellent theory−experiment fit (Pendry R factor[15] $R = 0.144$) as demonstrated in Figure 2b for a selected integer and a fractional-order beam. The best-fit values of the structure parameters are summarized in Table 1. Because of the huge accumulated database ($\Delta E \approx 10\,500$ eV) and the excellent fit quality, the limits of statistical errors are in the range of only 0.01−0.03 Å depending on the actual parameter.[14] This demonstrates the precision of today's quantitative LEED.

3. Hydrogen-Induced Restructuring of Ir(100)

As is well known, the reconstruction of clean surfaces as Ir(100) arises from the truncation of bonds by the creation of the surface. Equivalently, the reconstruction can (but must not) be lifted by restoring some surface bonding with adsorbing particles, so offering oxygen to Ir(100)-(5 × 1)-hex followed by annealing at suitable temperatures and reduction by hydrogen makes the surface reassume (1 × 1) the structure corresponding

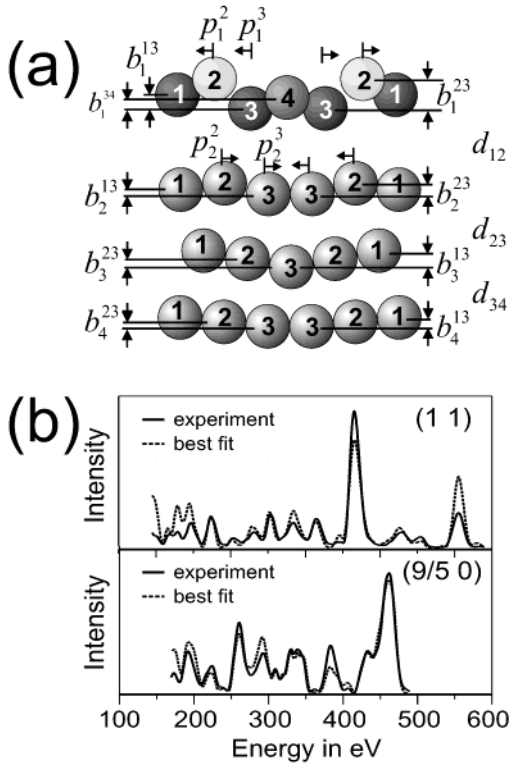

Figure 2. (a) Structural parameters of Ir(100)-(5 × 1)-hex. Quantities d_{ik} denote the smallest spacing between the subplanes of layers *i* and *k*. Atoms 2/6 and 3/5 denoted in Figure 1b were assumed to be symmetrically equivalent. (b) Experimental and best-fit calculated spectra compared for two selected beams.

TABLE 1: Structural Parameter Values of Ir(100)-5 × 1 According to Figure 2 as Determined by Quantitative LEED[a]

d_{12}	d_{23}	d_{34}	d_{45}	b_1^{13}	b_1^{23}	b_1^{34}	p_1^2	p_1^3
1.94	1.79	1.83	1.89	0.25	0.55	0.20	0.05	0.07
b_2^{13}	b_2^{23}	p_2^2	p_2^3	b_3^{13}	b_3^{23}	b_4^{13}	b_4^{23}	
0.07	0.10	0.01	0.02	0.10	0.05	0.06	0.03	

[a] All values are in angstroms.

to a metastable bulk termination.[16,17] The 20% extra atoms accommodated in the hexagonal layer are expelled to the surface, where they form rectangular islands residing on the now ordered substrate.[14]

However, the periodicity of the diffraction pattern remains when hydrogen is adsorbed on Ir(100)-(5 × 1)-hex.[18] Although there are only small intensity modifications for adsorption and annealing taking place with the sample kept below 180 K (indicating that the hex reconstruction is preserved), the intensities change dramatically when the sample temperature during adsorption and/or annealing is above that value. In the following text, we denote this phase as Ir(100)-(5 × 1)-hex-H. As displayed in Figure 3a, exposure to 50 L of hydrogen offered at about 300 K produces extra spots that are much weaker than in case of clean Ir(100)-(5 × 1)-hex. Whereas the average ratio between fractional- and integer-order spots is $r_{5\times1}^{\mathrm{hex}} \approx 0.6$ for Ir(100)-(5 × 1)-hex, the ratio is only $r_{5\times1}^{\mathrm{H}} \approx 0.04$ for Ir(100)-(5 × 1)-H. Also, the intensity spectra of the spots change substantially. Other (also weak) superstructures related to (5 × 1) develop when the adsorption conditions are modified. Seemingly streaky features along the superstructure spots as displayed in Figure 3b appear on exposure of Ir(100)-(5 × 1)-hex to 200 L of hydrogen at about 90 K, followed by annealing

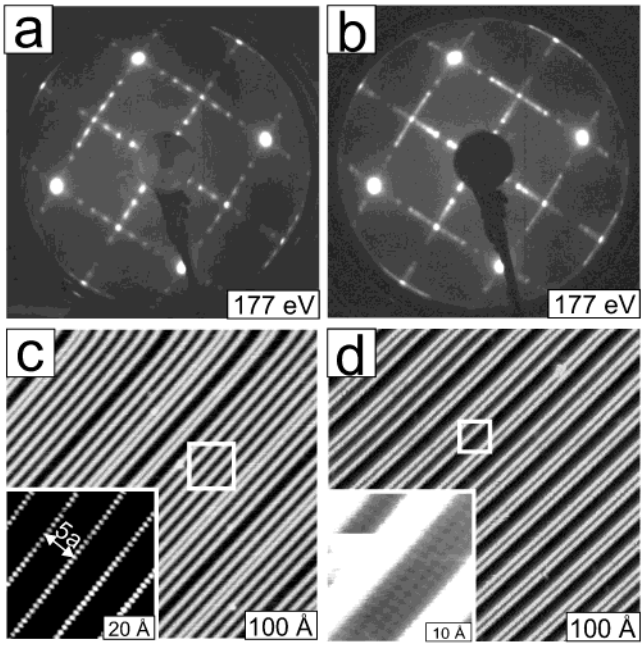

Figure 3. LEED patterns and STM images for (a, c) Ir(100)-(5 × 1)-H and (b, d) Ir(100)-(10 × 1)-H.

at about 300 K. Similar patterns have also been observed in other work and interpreted as a (3 × 1) superstructure.[19,20] The intensity analysis assuming a (3 × 1) reconstructed Ir(100) surface with an asymmetrically rumpled top layer covered by hydrogen led to a best-fit Pendry *R* factor of $R = 0.26$,[20] yet in our case, we find that the phase corresponds to a slightly disordered (10 × 1) superstructure, Ir(100)-(10 × 1)-H, with spots next to third-order positions being much stronger than others.[18] We will see below that this corresponds to a very different structure than that obtained in ref 20.

The reduced intensity of the extra spots as well as the strong modification of their spectra proves that the surface must have been restructured upon hydrogen deposition and assumed an atomic arrangement that is very different from the former quasi-hexagonal phase. Even though the superstructure spots are weak, they are still too strong to be caused by a mere hydrogen adatom structure (on an unreconstructed substrate), so a new arrangement of Ir atoms must occur. Yet, there is a huge number of possibilities that would cause a (5 × 1) superstructure (an even larger number for a (10 × 1) phase), and without a promising structural idea, one is lost. Here STM comes into play and proves to be invaluable because it fully provides the main features of the structures. Figure 3c displays the image of the (5 × 1)-H phase. Again there is a chainlike structure with, however, the lateral spacing of the chains being much larger than in the case of Ir(100)-(5 × 1)-hex. Except for occasional breaks, the spacing is 5*a*. The chains are of single-atomic width and height (i.e., single-atom Ir chains reside in almost ideal lateral (5 × 1) order on a (1 × 1) ordered Ir substrate). For the (10 × 1) phase, the chains are almost ideally arranged in a sequence of alternating 3*a* and 7*a* spacings corresponding to a (10 × 1) superstructure. Note that on average the spacing is again 5-fold with respect to the (1 × 1) unit cell dimension. The 7*a* spacing is large enough to allow the tip to dip between the chains, as shown in the inset of Figure 3d. Evidently, between the chains the surface is (1 × 1) ordered.

With this input, the structural analysis of Ir(100)-(5 × 1)-H (on which we concentrate) is almost routine. According to the model displayed in Figure 4a, the position of the chains above the surface and a chain-induced buckling within the otherwise

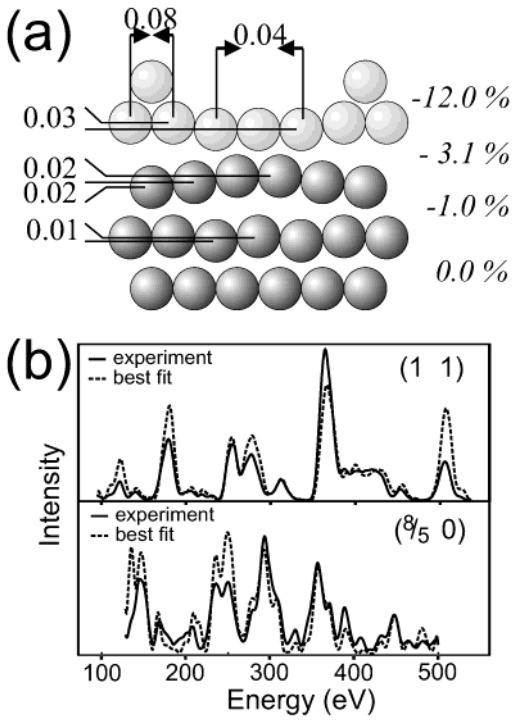

Figure 4. (a) Structural model and (b) comparison of experimental and best-fit calculated LEED spectra for Ir(100)-(5 × 1)-H. The percentages given for the changes in interlayer spacings in panel a refer to the bulk spacing of Ir(100), $d_b = 1.92$ Å.

(1 × 1)-ordered Ir substrate were allowed in the analysis, yielding the values indicated. Again the comparison between experimental and best-fit calculated LEED spectra is very good, as demonstrated for two selected beams in Figure 4b. It is obvious that hydrogen adsorption lifts the hexagonal reconstruction in a different way to that achieved by the above-mentioned oxygen adsorption. The 20% extra atoms within the top layer are also expelled to the surface, but there they arrange almost regularly as chains of single-atomic width. Obviously, every sixth chain of the former chains in the quasi-hexagonal arrangement is moved to the top of the surface. The remaining chains reassume (1 × 1) order, whereby some small buckling is induced by the new surface chains. The latter's length is huge, as apparent from large-scale STM images. It seems to be limited only by the size of the surface terraces (here ~1 μm), which in turn is limited by the accuracy of the surface alignment when the bulk sample is cut. The density and positions of hydrogen atoms at the surface remain unknown because neither STM nor quantitative LEED can "see" them in the present case. Concerning LEED, this is due to hydrogen's very weak scattering strength compared to that of Ir.

4. Epitaxial Nanowire Formation on Ir(100)

The Ir(100)-(5 × 1)-H phase presented in the last section is a real nanostructure because the lateral spacing of the Ir chains is $5a = 1.36$ nm. Therefore, one is tempted to use the phase as a template for the creation of additional nanostructures by the deposition of other atoms. In fact, the adsorption of iron, for example, leads to such structures, which will be demonstrated below. Figure 5 compares LEED intensity spectra of Ir(100)-(5 × 1)-H to those resulting by the additional deposition of Fe at two selected coverage values (about 0.4 and 0.8 ML Fe). Though the (5 × 1) periodicity of the surface is again saved, the spectra of the beams change markedly uponFe deposition. Of course, this is not surprising because there are additional

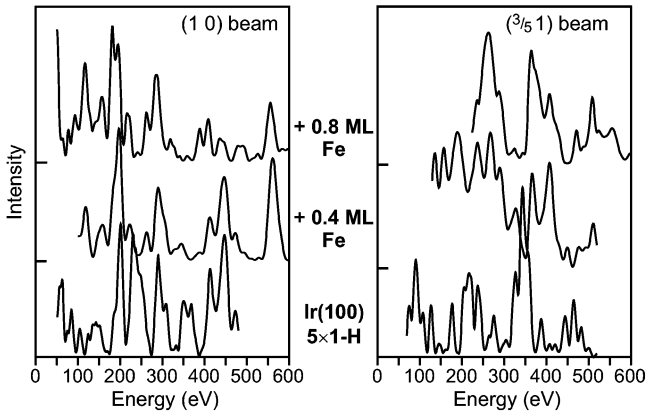

Figure 5. LEED intensity spectra of Ir(100)-(5 × 1)-H, Ir(100)-(5 × 1)-H+0.4 ML Fe and Ir(100)-(5 × 1)-H+0.8 ML Fe.

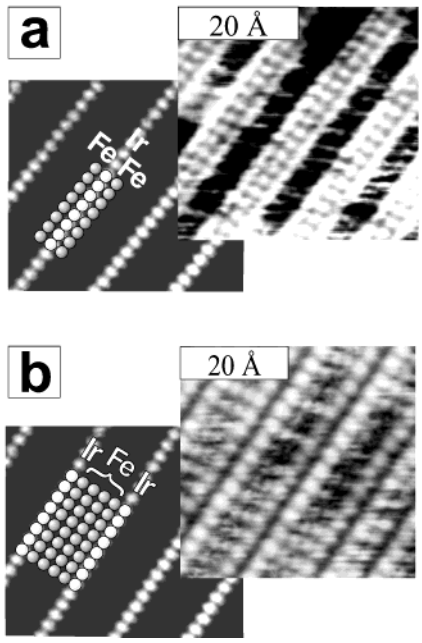

Figure 6. STM images of (a) Ir(100)-(5 × 1)-H+0.4 ML Fe and (b) Ir(100)-(5 × 1)-H+0.8 ML Fe. The image of the inset of Figure 3c is added in each case to illustrate the original monatomic Ir chains and their decoration by Fe.

(and coverage-dependent) contributions from the Fe atoms deposited. These contributions depend on the positions of the iron atoms, which are hidden in the spectra.

Again, the STM images of the two phases immediately reveal the type of applying surface model. As shown in Figure 6a, the iron atoms at 0.4 ML coverage have diffused to the monatomic Ir chains where they can form a maximum number of heterogeneous bonds. At the coverage displayed, practically all Fe atoms decorate the Ir chains, thus forming a periodic FeIrFe sandwich structure or, equivalently, a lateral {FeIrFe} superlattice. With further Fe deposition, the area between the sandwiches is filled by Fe so that eventually an {Fe_4Ir} superlattice results, as displayed in Figure 6b.

The reader should note that whereas for the {FeIrFe} phase Ir and Fe chains appear at the same height in the STM image the Ir chains seem to be pushed into the surface relative to the Fe chains (or even missing) in the {Fe_4Ir} superlattice. Yet in view of the larger covalent radius of Ir compared to that of Fe (1.36 vs 1.24 Å), this is most likely due to an electronic effect

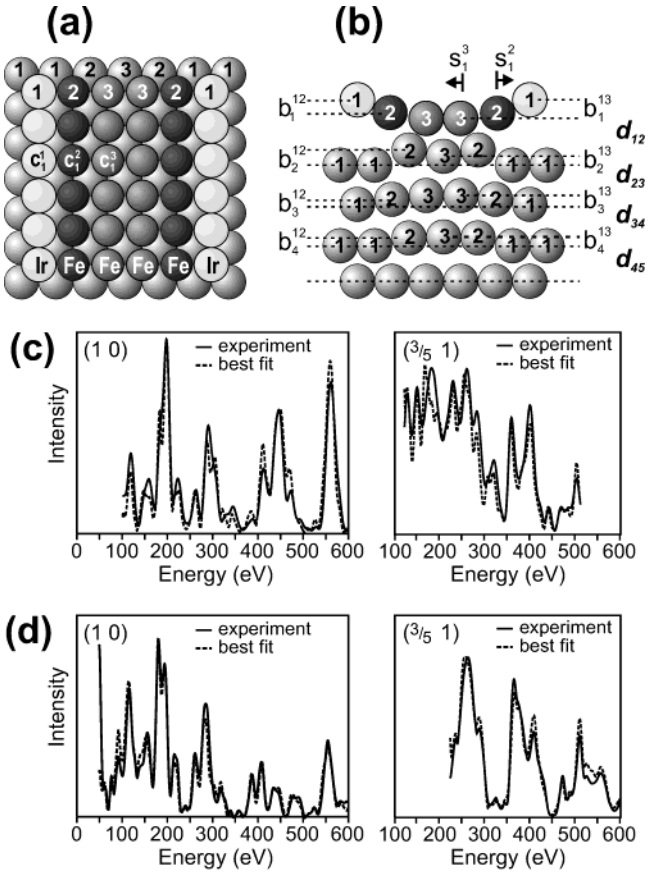

Figure 7. Ball model in (a) top and (b) side views accounting for the {FeIrFe} and {Fe_4Ir} superlattices displayed in Figure 6. Below, experimental and calculated best-fit spectra for a selected beam are compared for (c) {FeIrFe} and (d) {Fe_4Ir}.

TABLE 2: Parameter Values Determined for the {FeIrFe} and {Fe_4Ir} Superlattices According to the Model Displayed in Figure 7[a]

	d_{12}	d_{23}	d_{34}	d_{45}	c_1^1	c_1^2	c_1^3	c_1^2	c_1^3
$c_1^3s_1^2s_1^3$ {FeIrFe}	1.65	1.89	1.86	1.92	0	90	10	0.04	n.a.
{Fe_4Ir}	1.67	1.91	1.89	d_b(fix)	0	100	90	0.05	0.03

	b_1^{12}	b_1^{13}	b_2^{12}	b_2^{13}	b_3^{12}	b_3^{13}	b_4^{12}	b_4^{13}
{FeIrFe}	0.11	0.16	0.05	0.04	0.05	0.07	0.01	0.01
{Fe_4Ir}	0.10	0.11	0.09	0.02	0.03	0.03	n.a.	n.a.

[a] Quantities d_{ik} correspond to spacings between the nearest subplanes of layers *i,k* (bulk value: $d_b = 1.92$ Å). All values are in angstroms except for quantities c_i^k, which are in percent.

because both kind of atoms should reside in 4-fold hollow sites of the substrate. This (and other crystallographic quantities, in particular, those for deeper layers) can be retrieved by quantitative LEED analyses of both phases. Again guided by the STM images, we used the model displayed in Figure 7 as it applies to both superlattices when the concentrations c_1^i of Fe atoms in rows i are varied to allow for vacancies on sites $i = 2, 3$. For sites $i = 1$, a potential intermixing of Ir and Fe was tested.[21] A very good fit between experimental and calculated model spectra results, as demonstrated in Figure 7. Table 2 shows that by the values of c_1^i being either close to zero or to 100%, the chemical order (i.e., the occupation of sites according to the ideal {FeIrFe} and {Fe_4Ir} superlattice models) is very good. Also, with $b_1^{12} \approx 0.1$ Å in both phases, the Ir rows protrude from the surface, as expected from the atomic radii. This proves that the STM appearance is indeed a mere electronic effect.

5. Conclusions

By the examples presented, we have demonstrated that the combination of STM and LEED is a powerful tool for the structural investigation of surfaces. They are not only complementary in the sense that they probe real and reciprocal space but they also access surface structures to a different precision and depth. In principle, the LEED intensities contain all of the structural information, but it is hidden by the loss of the diffraction amplitude's phase and by multiple scattering. Also, LEED can retrieve the correct structure only if all relevant structural parameters are varied and their best-fit values are eventually determined. In other words, from LEED either complete structural information can be extracted or no reliable atomic coordinates at all result. If one starts with the wrong model type, there will never be a satisfying theory−experiment fit. However, because there is always a best fit, one might be tempted to ignore its unsatisfying level and so misinterpret the result as the true structure. Yet, with atomically resolved STM applied in parallel (i.e., for the same surface phase), this risk is minimized, and the applicable model type can be determined in most cases. In this sense, STM can be the key to surface structure.

Nevertheless, proper care should always be exercised. As demonstrated for the case of Ir(100)-(5 × 1)-hex, the quasi-hexagonal model of the surface is not obvious from STM, but many other types of surface models can be excluded. Moreover, besides the scanned image being structurally incomplete, the STM may also occasionally give a wrong impression of the atomic arrangement in the top layer, so in the above example of the {Fe_4Ir} superlattice, the Ir chains appeared as dark lines. In the worst case, this could have been misinterpreted as a missing row or at least as a row structurally depressed with respect to the neighboring rows. Another case that we recently encountered is that of the Pt(110)-c(2 × 2)-Br phase. Its STM image had originally been interpreted as being due to a c(2 × 2) chemical superstructure in which Br atoms had been substituted for Pt atoms,[22] but the LEED analysis failed to produce a satisfying fit for this model type and instead established that a c(2 × 2) adatom model is correct, which was confirmed by DFT calculations.[23] This means that LEED is able to realize when it is put on the wrong structural track, at least if one refuses to be satisfied with a low-quality theory−experiment fit, so the combined application of STM and LEED is almost ideal: The atomically resolved STM image provides a starting point for the structural search, which is applied by LEED to fit the experimental intensities by model calculations. If this starting point happens to be wrong because of a structural misinterpretation of the STM image, then LEED becomes aware of that, and a reinterpretation of the STM image might allow for a new start.

Acknowledgment. We are indebted to the Deutsche Forschungsgemeinschaft for financial support.

References and Notes

(1) Spišák, D.; Hafner, J. *Surf. Sci.* **2003**, *546*, 27.

(2) Hammer, L.; Meier, W.; Schmidt, A.; Heinz, K. *Phys. Rev. B* **2003**, *67*, 125422/1.

(3) Seubert, A.; Heinz, K.; Saldin, D. K. *Phys. Rev. B* **2003**, *67*, 125417/1.

(4) Special issue on holographic and other direct methods for surface structures using electrons and photons. Heinz, K., Guest Ed. *J. Phys.: Condens. Matter* **2001**, *13*(47).

(5) Watson, P. R.; Van Hove, M. A.; Hermann, K. *NIST Surface Structure Data Base*, version 4.0; National Institute of Standards and Technology: Gaithersburg, MD, 2001.

(6) Heinz, K. *Prog. Surf. Sci.* **1995**, *58* 637.
(7) Blum, V.; Heinz, K. *Comput. Phys. Commun.* **2000**, *134*, 392.
(8) Ignatiev, A.; Jones, A. V.; Rhodin, T. N. *Surf. Sci.* **1972**, *30*, 573.
(9) Van Hove, M. A.; Koestner, R. J.; Bibérian, P. C.; Kesmodel, L. L.; Bartos, I.; Somorjai, G. A. *Surf. Sci.* **1981**, *103*, 189.
(10) Lang, E.; Müller, K.; Heinz, K.; Van Hove, M. A.; Koestner, R. J.; Somorjai, G. A. *Surf. Sci.* **1983**, *127*, 347.
(11) Moritz, W.; Müller, F.; Wolf, D.; Jagodzinski, H. *Abstract Book of the 9th Vacuum Congress and 5th International Conference on Solid Surfaces*, Madrid, 1983; p 70.
(12) Bickel, N.; Heinz, K. *Surf. Sci.* **1985**, *163*, 435.
(13) Johnson, K.; Ge, Q.; Titmuss S.; King, D. A. *J. Chem. Phys.* **2000**, *112*, 10460.
(14) Schmidt, A.; Meier, W.; Hammer, L.; Heinz, K. *J. Phys.: Condens. Matter* **2002**, *14*, 12353.
(15) Pendry, J. B. *J. Phys. C* **1980**, *13*, 937.
(16) Küppers, J.; Michel, H. *Appl. Surf. Sci.* **1979**, *3*, 179.
(17) Heinz, K.; Schmidt, G.; Hammer, L.; Müller, K. *Phys. Rev. B* **1985**, *32*, 6214.
(18) Hammer, L.; Meier, W.; Klein, A.; Landfried, P.; Schmidt, A.; Heinz, K. *Phys. Rev. Lett.* **2003**, *91*, 156101.
(19) Moritani, K.; Okada, M.; Kasia, T.; Murata, Y. *Surf. Sci.* **2000**, *445*, 315.
(20) Sauerhammer, B.; Johnson, K.; Greenwood, C.; Braun, W.; Held, G.; King, D. A. *Surf. Sci.* **2001**, *488*, 154.
(21) Klein, A.; Schmidt, A.; Hammer, L.; Heinz, K. *Europhys. Lett.* **2004**, *65*, 830.
(22) Swamy, K.; Hanesch, P.; Sandl, P.; Bertel, E. *Surf. Sci.* **2000**, *466*, 11.
(23) Blum, V.; Hammer, L.; Heinz, K.; Franchini, C.; Redinger, S.; Swamy, K.; Deisl, C.; Bertel, E. *Phys. Rev. B* **2002**, *65*, 165408.